A Multicomponent Blend as a Diesel Fuel Surrogate for Compression Ignition Engine Applications

Yuanjiang Pei[1]
Transportation Technology R&D Center,
Argonne National Laboratory,
Argonne, IL 60439
e-mail: ypei@anl.gov

Marco Mehl
Chemical Sciences Division,
Lawrence Livermore National Laboratory,
Livermore, CA 94550

Wei Liu
Chemical S&E Division,
Argonne National Laboratory,
Argonne, IL 60439

Tianfeng Lu
Department of Mechanical Engineering,
University of Connecticut,
Storrs, CT 06269

William J. Pitz
Chemical Sciences Division,
Lawrence Livermore National Laboratory,
Livermore, CA 94550

Sibendu Som
Transportation Technology R&D Center,
Argonne National Laboratory,
Argonne, IL 60439

A mixture of n-dodecane and m-xylene is investigated as a diesel fuel surrogate for compression ignition (CI) engine applications. Compared to neat n-dodecane, this binary mixture is more representative of diesel fuel because it contains an alkyl-benzene which represents an important chemical class present in diesel fuels. A detailed multicomponent mechanism for n-dodecane and m-xylene was developed by combining a previously developed n-dodecane mechanism with a recently developed mechanism for xylenes. The xylene mechanism is shown to reproduce experimental ignition data from a rapid compression machine (RCM) and shock tube (ST), speciation data from the jet stirred reactor and flame speed data. This combined mechanism was validated by comparing predictions from the model with experimental data for ignition in STs and for reactivity in a flow reactor. The combined mechanism, consisting of 2885 species and 11,754 reactions, was reduced to a skeletal mechanism consisting 163 species and 887 reactions for 3D diesel engine simulations. The mechanism reduction was performed using directed relation graph (DRG) with expert knowledge (DRG-X) and DRG-aided sensitivity analysis (DRGASA) at a fixed fuel composition of 77% of n-dodecane and 23% m-xylene by volume. The sample space for the reduction covered pressure of 1–80 bar, equivalence ratio of 0.5–2.0, and initial temperature of 700–1600 K for ignition. The skeletal mechanism was compared with the detailed mechanism for ignition and flow reactor predictions. Finally, the skeletal mechanism was validated against a spray flame dataset under diesel engine conditions documented on the engine combustion network (ECN) website. These multidimensional simulations were performed using a representative interactive flame (RIF) turbulent combustion model. Encouraging results were obtained compared to the experiments with regard to the predictions of ignition delay and lift-off length at different ambient temperatures.

1 Introduction

Predictive chemical kinetic models for fuels are needed so that the effect of fuel composition on engine performance can be assessed. These chemical kinetic models need to be computationally efficient to make engine simulations tractable. However, transportation fuels, such as gasoline and diesel, contain hundreds of components. Rather than developing a mechanism for all these components, representative surrogates are usually chosen that consider only a small number of representative components. Even so, detailed chemical kinetic models for fuel surrogates are often quite large, consisting of thousands of species and reactions. These large detailed chemical kinetic mechanisms need to be reduced in size for use in multidimensional engine simulations. Various reduction techniques have made this possible, while maintaining high chemical fidelity [1]. The large extents of reductions enable the inclusion of more components in a fuel surrogate to better mimic the real fuel properties in engine simulations. Together with the development in high-performance computing (HPC) capability, complex chemistry can now be applied for large-scale practical engine simulations.

Previously, the authors have developed a reduced mechanism for a single-component diesel surrogate, i.e., neat *n*-dodecane to be used in engine simulations [2]. The primary goal of this study is to develop a reduced mechanism for a two-component surrogate consisting of *m*-xylene and *n*-dodecane for multidimensional CI engine simulations. This blend is considered to be more representative of diesel fuel than a neat *n*-dodecane surrogate because it contains an alkyl-benzene, which represents an important chemical class present in diesel fuels. In this study, a detailed mechanism for xylene was first validated by comparison with fundamental experimental combustion data. Then the xylene mechanism was combined with a previously developed mechanism for *n*-dodecane. This combined detailed mechanism was first reduced using the state-of-the-art reduction techniques. The reduced mechanism was then validated against the detailed mechanism and available experimental data from a ST and flow reactor. Finally, the mechanism was further validated using a spray flame dataset relevant to typical diesel engine conditions, including both nonreacting and reacting conditions with the focus on the study of liquid length, vapor penetration length, ignition delay, lift-off length, and soot.

The paper is organized in the following way. The methodology for assembling and validating the detailed reaction mechanism is presented first, followed by the mechanism reduction procedure. The reduced mechanism is then validated against 3D spray combustion data available in the literature. The sooting propensity for these mixtures was also assessed. Some conclusions were derived at the end.

2 The Kinetic Mechanism

A kinetic mechanism describing the oxidation of *n*-dodecane/*m*-xylene mixture was assembled based on recently published kinetic mechanisms developed by the Lawrence Livermore National

[1] Corresponding author.

Contributed by the Combustion and Fuels Committee of ASME for publication in the Journal of Engineering for Gas Turbines and Power. Manuscript received February 27, 2015; final manuscript received March 3, 2015; published online May 12, 2015. Editor: David Wisler.

Laboratory. The detailed multicomponent mechanism for *n*-dodecane and *m*-xylene was developed by combining the previously developed *n*-dodecane mechanism [3] with a recently developed mechanism detailing the combustion of the xylene isomers [4].

The two parent mechanisms were individually validated against an extensive set of experimental data for both fuels, including ignition delay time, speciation, and laminar flame speed data. While the comparisons pertaining to the validation of the *n*-alkane mechanism can be easily accessed in the literature [3,5], the description of the xylene mechanism [4] and its validation are not readily available to the readers; therefore, a short description of the main features of the mechanism together with validation comparisons is reported here.

The general structure of the mechanisms obeys to the hierarchical criteria: fuel specific modules are built on top of the core chemistry constituted by the reaction mechanism of C1–C4 species. Large molecule mechanisms include the reaction pathways of all the lighter components formed during the decomposition and oxidation of the fuel molecule: chemical model for benzene and toluene oxidation represents a submodel of all the heavier alkyl aromatics. The toluene mechanism included in the LLNL gasoline surrogate mechanism and the core chemistry associated with it [6] constitutes the submodels of choice for the lighter aro-matics and has been used to derive the reaction rates applied to the xylene isomers. The reaction rate constants adopted for toluene, which were obtained from previous works, including experimental and modeling studies [7–10], have been generalized for xylenes to account for the different numbers and positions of methyl groups present in the fuel molecule.

In the case of xylenes, however, the presence of multiple side-chains induces additional reaction pathways affecting the reactivity of the fuels. ST and RCM experiments highlighted that the reactivities of para- and meta-xylene are quite similar, while ortho-xylene ignites significantly faster than the other two isomers [11]. This characteristic behavior derives from the proximity of the two alkyl chains that allows for hydrogen transfers between the two methyl groups and some limited low temperature reac-tions [12]. Few mechanisms accounting for these low temperature pathways are available in literature [12].

The existence of oxidation pathways specific to ortho-xylene necessitates the development of a dedicated submechanism for this isomer. The present version of our mechanisms includes the low temperature chemistry specific to ortho-xylene, and all the chemical species deriving from its benzyl radicals are treated in a detailed way. Figure 1 summarizes the low temperature pathways for ortho-xylene in the mechanisms discussed in this paper.

Ortho-xylene radicals can undergo oxygen addition and, because of the weak benzyl C–H bond, quickly isomerize to hydroperoxymethyl-benzyl radicals. The aromatic resonance allows the migration of the radical site to the carbon adjacent to the COOH group (Fig. 1) allowing for HO_2 elimination and the formation of C_8H_8. This pathway becomes dominant when the temperature exceeds 800 K. The formation of cyclic ethers is also possible and competes with the second O_2 addition. A second H transfer finally leads to the formation of the ketohydroperoxides. It should be noted that, even though the isomerization steps are favored by the weak C–H bond, the resonance inhibits the O_2 addition steps resulting in a low activation energy for the decomposition of the R–O_2 radical (21 kcal), limiting the effectiveness of the degenerate branching path described herein.

These reaction pathways are not possible for para- and meta-xylene, since the two methyl groups are far apart. In this preliminary version of the mechanism, these two isomers were not differentiated since the chemistry of their consumption follows very similar steps. It was assumed that the same mechanism can predict all the major combustion features reasonably well. Moreover, since the high temperature processes involving the attack on the ring are scarcely selective on the H atoms on the ring, the different methyl-phenyl radicals were not differentiated either for the

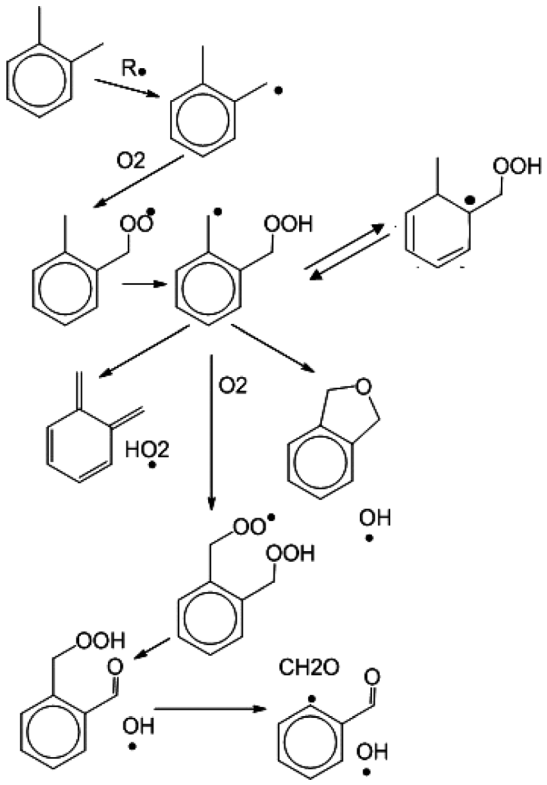

Fig. 1 Low temperature oxidation of ortho-xylene

three isomers: once a methyl-phenyl radical is formed, the same sequence of reactions described in the mechanism for toluene follows.

The xylenes mechanism has been validated for a wide range of experimental data for ignition from low and high temperature, a jet stirred reactor, and spherically propagating flames.

The first set of comparisons involves the ignition behaviors of these fuels in ST and RCM experiments. Shen and Oehlschlaeger [11] measured the ignition delay times of different C_8H_{10} aromatics/air mixtures in a ST at moderate temperatures (950–1400 K) and high pressures (10–40 atm) (Fig. 2).

Ignition data for ethylbenzene are also shown as a reference. The model correctly reproduces this behavior showing a satisfactory agreement with the experimental data. Compared to the other xylenes, the higher reactivity of the ortho-isomer is more evident at lower temperature, where the O_2 addition and HO_2 elimination

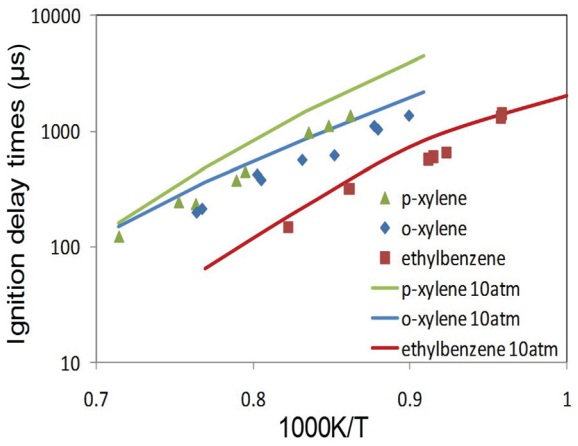

Fig. 2 Validation of the mechanism of C_8 aromatics against ST experiments [5] (10 atm in stoichiometric fuel–air mixtures)

are still active. In order to validate the low temperature submechanism specific to ortho-xylene, Fig. 3 compares calculated results with a set of RCM data collected by Roubaud et al. [12] at conditions similar to the ones considered by Shen (14–19 atm), except that the O_2 molar percentage in the synthetic air has been altered from 21% to 27% to enhance the low temperature reactiv-ity of the fuel.

The calculations predict a slight negative temperature coefficient behavior similar to that seen in the experiments. The model provides a good agreement with the data with the exception of the lowest temperatures, where the calculations underpredict the ignition delay times. It should be mentioned, however, that in the simulations the heat loss model was not calibrated using unreactive pressure traces as is usually done for RCM simulations [13], since the pressure traces were not available. A heat loss model based on the volume history profile in Ref. [6] from a similar set of data obtained in the same device was used here to account for the heat loss effect in the RCM data. This approach provides a qualita-tively correct description of the ignition experiments, but does not allow a precise quantification of heat transfer contribution, which can be important at long ignition delay times. The overall agree-ment supports the general validity of the mechanism.

The first two sets of comparisons confirmed the ability of the mechanism in predicting ignition behavior of these C_8 alkyl-aromatics. Another test which specifically validates the reaction pathways in the model comes from speciation data. Mechanism predictions have been compared with jet stirred reactor data published by Gail and Dagaut [14], who tested the oxidation of the para-xylene between 900 K and 1400 K, 1 atm and different equivalence ratios.

Figure 4 shows the comparison at $\phi = 1$. The model reproduces well the measured species profiles not only in terms of the final products but also for some important intermediates (benzalde-hyde, benzene, and toluene). Not surprisingly, toluene and ben-zene are two major products, since the oxidation of the side chains is the dominant process at the early stage of combustion. The cor-rect prediction of small hydrocarbons supports the general validity of the submodel relative to the oxidation of the ring.

An additional comparison involves flame speeds of three different aromatic species: toluene, meta-xylene, and ethylbenzene (Fig. 5). Johnston and Farrell [15] measured laminar flame speeds for toluene, ethylbenzene, and xylene at elevated temperature and pressure (450 K, 3 atm). The flame speed was determined using high speed Schlieren visualization, used to monitor the flame growth following the ignition. The data are corrected for flame stretch to determine the unstretched laminar burning velocities. The model provides satisfactory predictions, reproducing correctly the trends highlighted by the experiments.

The final mechanism obtained combining the *n*-alkanes and xylenes models consists of 2885-species and 11,754 reactions.

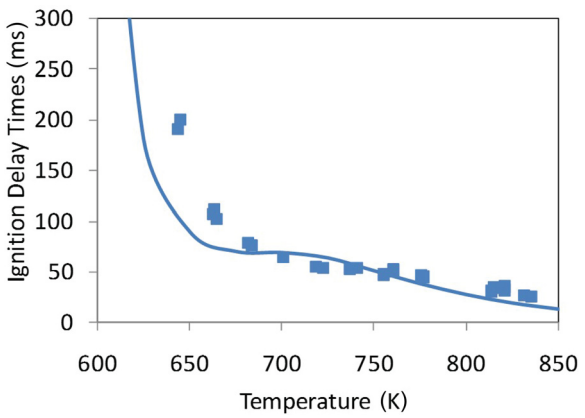

Fig. 3 Ortho-xylene autoignition in a RCM at 14–19 atm, ϕ = 1,[O_2]/[inert] = 0.37. Symbols: data [12], line: calculations.

Due to the primary importance of ignition delay, time predictions in the context of this study, some ST comparisons are shown in Fig. 6.

The ST data obtained by Shen and Oehlschlaeger [11] at 10 and 40 bar and $\phi = 0.5$ and 1.0 are accompanied by the ignition delay times of *n*-dodecane measured at about 20 bar and the same equivalence ratios by Vasu et al. [16]. Since the xylene data were originally collected at 10 and 40 bar, in order to allow a direct comparison between the two fuel components the ignition delay times were normalized to 20 bar using a $\tau_{ign} - 1/P$ scaling. The model reproduces the ignition delay times of the two fuel components with reasonable accuracy.

Unfortunately, very limited datasets are available to validate the mechanism for the mixture investigated in this study, particularly for the low temperature conditions. In a previous work by Natelson et al. [17], an *n*-dodecane/*m*-xylene mixture analogous to the one considered in this study (77/23 vol. %) was tested in the Drexel University pressurized flow reactor at lean conditions ($\phi = 0.23$).

The initial fuel concentration in that study was only 460 ppm. Figure 7 compares the CO profile measured by Natelson against the mechanism predictions. Again, the model fairly characterizes the partial oxidation in the low temperature region reproducing with good accuracy the magnitude of the CO peak. The predicted peak location is shifted lower with respect to the measured locations by about 40 K. This discrepancy is likely related to a slight overestimation of *n*-dodecane reactivity at lean conditions in the low temperature region, consistent with the ignition delay time comparison shown in Fig. 6.

3 Mechanism Reduction

In order to reduce this mechanism, two rounds of DRG-X [18] and DRGASA together with one round of isomer lumping were performed. These reduction methods have been applied to a variety of applications to obtain reduced mechanisms and satisfactory results were achieved [19–22]. The current reduction was based on sampling simulations of ignition delay using SENKIN [23] and extinction temperature profiles using a perfectly stirred reactor (PSR), for a mixture (denoted as SR23) of 77% of *n*-dodecane ($nC_{12}H_{26}$) and 23% *m*-xylene (M-XYL), at pressure of 1–80 bar, equivalence ratio of 0.5–2.0, and initial temperature of 700–1600 K for SENKIN and inlet temperature of 300 K for PSR. The detailed mechanism was used as a benchmark in the sampling simulations and sampling simulations using the reduced mecha-nisms were compared to this benchmark to aid in the reduction.

The reduction flow diagram is shown in Fig. 8. Details of the reduction strategies and the error tolerances used could be found in Refs. [18] and [19]; thus, were only briefly described here. DRG-X was adopted instead of DRG due to its ability for species-specific error control, which allows the specifications of different error tolerances for different species and heat release rate. This led to the derivation of smaller skeletal mechanisms, while maintain-ing similar chemical fidelity. In the first round of reduction with DRG-X, the error tolerance for heat release and H radical were chosen to be 0.1 and 0.3, respectively. The error tolerance for the other species used the default value 0.5. This procedure reduced the detailed mechanism to a skeletal mechanism with 449 species and 2098 reactions. After this, DRGASA was applied to obtain a mechanism with 227 species and 1063 reactions. This mainly eliminated the species that did not significantly affect the global target parameters, including ignition delays and extinction temperature profiles in PSR. Then, isomer lumping was performed to further reduce the mechanism to 202 species. Thirteen pairs of isomers were grouped into lumped species designated in Table 1. Finally, the methods of DRG-X and DRGASA were applied for the second round to further reduce its size, and finally a skeletal mechanism with 163 species and 887 reactions was obtained.

Figure 9 shows a comparison between the predicted ignition delay times for a broad range of conditions ($P = 1$, 5, 10, 20, 40,

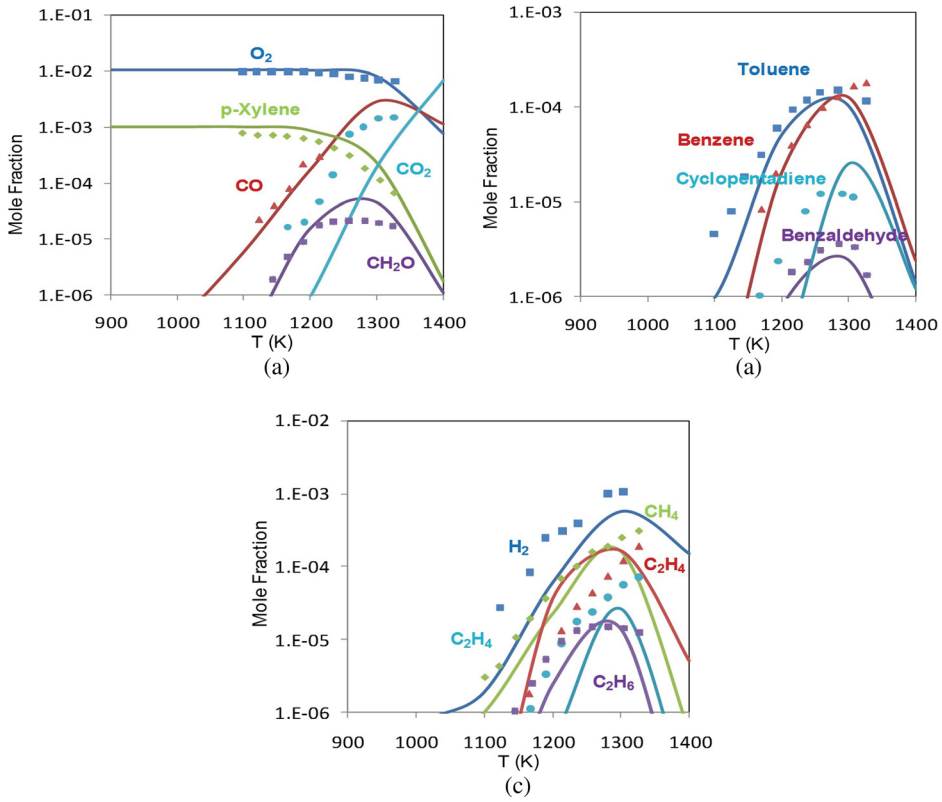

Fig. 4 Oxidation of para-xylene in a jet stirred reactor at 1 atm, $\phi = 1$, 1000 PPM fuel, and 0.1 s residence time. Symbols: data [13], lines: calculations.

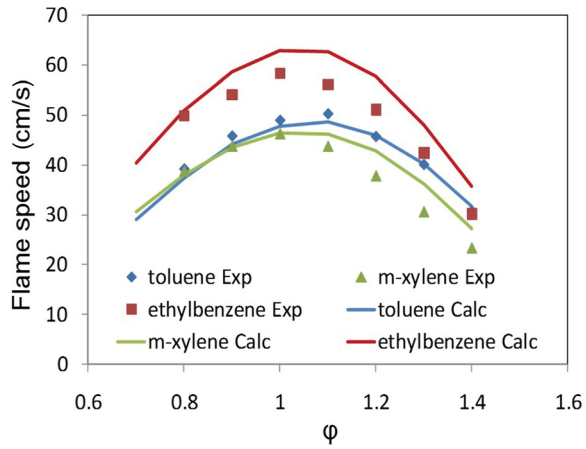

Fig. 5 Flame speeds of toluene, meta-xylene and ethyl benzene at 350 K and 3 atm. Symbols: data [14], lines: calculations.

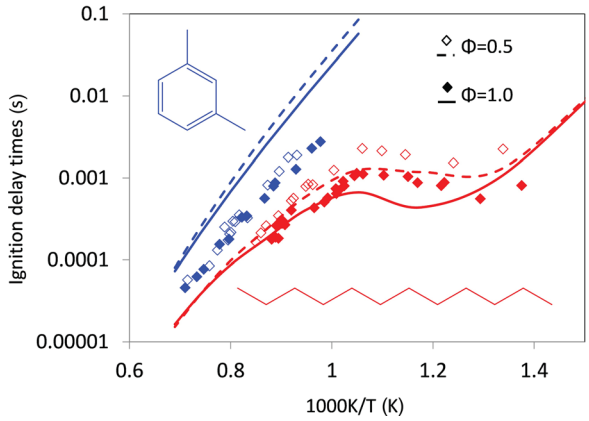

Fig. 6 Predicted (lines) and experimental [11,15] ignition delay times of the two surrogate fuel components at 20 bar. *m*-Xylene data [11] are normalized to 20 bar assuming a $\tau_{ign} - 1/P$ scaling.

and 80 bar) relevant to engines, obtained using the detailed kinetic mechanism and the reduced one. The close match between the detailed and reduced mechanisms supports the use of the reduced mechanism for engine simulations.

4 Comparison Against 3D Spray Combustion Dataset

The spray flame dataset [24,25] is obtained from the ECN [26], which is a platform for model development and validation at engine relevant conditions [27–47]. The 3D calculations were performed in a commercially available CFD code named CONVERGE [48]. The computational domain is a constant-volume, cubic combustion chamber with dimensions of 108 mm. Some boundary conditions are listed in Table 2. The details of the computational models can be found in a previous study [44], and hence will only be briefly discussed here. The traditional Lagrangian discrete phase model along with the blob injection method [49] was used to treat the liquid spray. The liquid mixture properties for *n*-dodecane and *m*-xylene were obtained from National Institute of Standards and Technology (NIST) [50]. The droplet secondary breakup and collision processes were modeled using Kelvin–Helmholtz and Rayleigh–Taylor model [51,52] and no time counter algorithm [53], respectively. The droplet evaporation was accounted for by using Frossling correlation [54]. Dynamic drag model [55] was used to model the droplet drag. The renormalization group k-ε turbulence model [56] was used to simulate the turbulence. A Hiroyasu-based soot model [57] was used, which assumes that the mass production of soot within a computational cell was determined from a single-step competition between

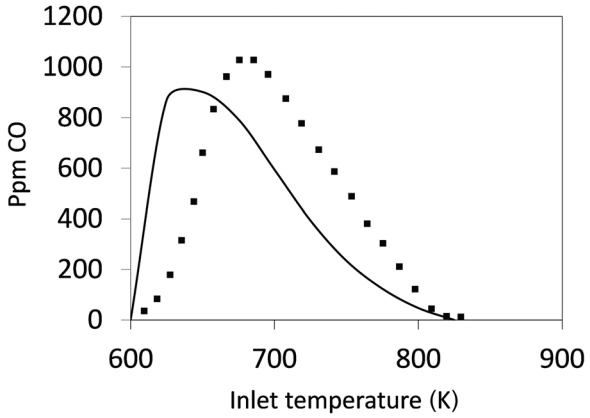

Fig. 7 Predicted (line) and experimental (symbols) [16] CO profiles for the two-component surrogate (SR23) in the Drexel pressurized flow reactor: $P = 8$ bar, $\tau = 110$ ms, $\phi = 0.23$

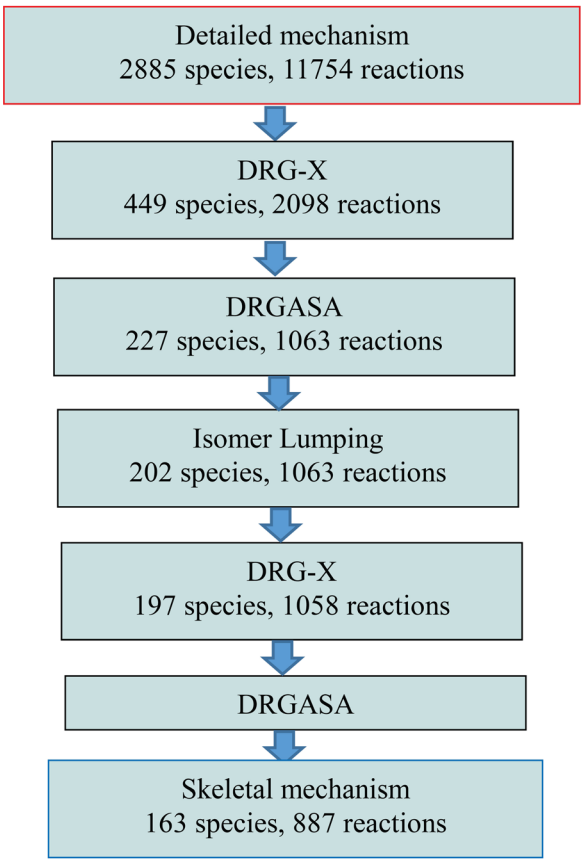

Fig. 8 Mechanism reduction flow diagram

formation and oxidation rates. The soot formation rate depends on the formation of C_2H_2 species, which is a precursor for soot production. Soot oxidation is modeled using Nagle and Strickland-Constable correlations [58] assuming the soot particles to be spherical and uniform in size.

The RIF [59] combustion model, which considers turbulence–chemistry interactions by assuming a presumed beta PDF for scalars, was coupled to a 3D unsteady Reynolds-averaged Navier–Stokes solver. The authors recently implemented and tested the RIF implementation for *n*-dodecane fuel under ECN conditions [44], and this work is intended to extend the RIF implementation approach to multicomponent fuels. Simulations were performed at a HPC cluster at Argonne National Laboratory following the best practices as in a previous study [44].

The skeletal multicomponent mechanism developed was validated by comparing against the available experimental results for both single (*n*-dodecane) and multicomponent (*n*-dodecane and *m*-xylene) fuels under diesel engine conditions. All the simulation results are based on this skeletal multicomponent mechanism and the calculations for neat *n*-dodecane were performed by simply setting the percentage of *m*-xylene to zero in the simulations.

The nonreacting case was first studied with the focus on the liquid and vapor penetration lengths. Figure 10 presents the comparison of experimental and computed liquid length at 900 and 1000 K ambient temperature conditions. The liquid length in the simulations is defined as the distance from the nozzle tip to the furthest axial location of 99% liquid fuel mass surface contour. One can see that the computed liquid lengths are in good agree-ment with the experiments, although slightly under-prediction at early times is found for the 900 K ambient condition. The vapor penetration length, defined as the distance from the nozzle to the axial boundary of 3% fuel vapor mass fraction near the head of the vapor plume in the simulations, is reported in Fig. 11 at 900 K condition. Excellent prediction is observed compared to the measurement.

After the nonreacting baseline condition was validated, the reacting cases were studied focusing on ignition delay, lift-off length, and soot predictions for both neat *n*-dodecane and the SR23 mixture. The comparison of ignition delay for SR23 and *n*-dodecane from both experiments and computations is reported in Fig. 12(*a*) at different ambient temperatures. In the simulation, ignition delay was defined as the duration from the start of injec-tion to the time of maximum rate of peak temperature rise. It can be seen that very good predictions were obtained for both SR23 and *n*-dodecane compared to the available experimental results at different ambient temperatures. From the experimental data, it is noted that addition of *m*-xylene slows down the reactivity and delays ignition, being consistent with the fact that SR23 has a lower cetane number of 70 [24] compared to *n*-dodecane of 87 [25]. The simulations captured this trend very well at all the ambient temperatures demonstrating its ability to capture the slower reactivity trends for the mixtures. The longer ignition delay of the SR23 mixture compared to that of neat *n*-dodecane allows more time for fuel–air mixing before the start of combustion. Also, the reduced mechanism can quantitatively capture the ignition delay values for both SR23 and pure *n*-dodecane. However, the sensitivity of ignition delay to fuel composition going from neat *n*-dodecane to the binary mixture is slightly under-predicted as shown in Fig. 12(*a*).

Figure 12(*b*) presents the predicted lift-off lengths for SR23 and *n*-dodecane compared to experimental results at different am-bient temperatures. Figure 13 presents the corresponding contours plots at 1.5 ms for 900 K and 1000 K ambient conditions for the SR23 mixture. The white line denotes the flame lift-off length location and the ignition delay values are also reported. The experimental definition of lift-off length used the distance from nozzle tip to the location of 50% of OH* leveling off value aver-aged over the quasi steady-state [26]. In the present simulation, the lift-off length was defined based on OH mass fraction due to the absence of species OH* in the kinetic model, and was defined as the distance from the nozzle exit to the point, where the OH mass fraction reaches 14% of its maximum during the quasi steady-state portion of the simulation. This definition is based on the recommendations from the ECN-2 workshop [60]. The choice of 14% threshold is more consistent with the experimental defini-tion based on the 0D [61] and 2D [33] studies comparing OH and OH*. From Fig. 12(*b*), it can be seen that the lift-off lengths of neat *n*-dodecane at different ambient temperatures can be pre-dicted well. However, under-predictions were observed for SR23, especially at lower ambient temperatures. Simulations can capture the effect of longer lift-off length when *m*-xylene is added to *n*-dodecane. This also indicates that the fuel–air mixing will be

Table 1 List of isomer groups with mole fractional amounts of each of isomer in the group

Group	Isomers
ISO1	C12OOH4-6O2 (0.4074); C12OOH3-5O2 (0.1855); C12OOH4-2O2 (0.4071)
ISO2	C12OOH5-7O2 (0.2949); C12OOH5-3O2 (0.2951); C12OOH6-4O2 (0.2047); C12OOH6-8O2 (0.2054)
ISO3	C12H25O2-6 (0.4107); C12H25O2-5 (0.5893)
ISO4	C12H25O2-3 (0.2610); C12H25O2-4 (0.7390)
ISO5	C12OOH4-6 (0.4070); C12OOH3-5 (0.1862); C12OOH4-2 (0.4067)
ISO6	C12OOH5-7 (0.2894); C12OOH5-3 (0.2899); C12OOH6-4 (0.2103); C12OOH6-8 (0.2104)
ISO7	C12OOH6-9 (0.4086); C12OOH5-8 (0.5914)
ISO8	C12H25-6 (0.1605); C12H25-4 (0.6607); C12H25-5 (0.1788)
ISO9	C12KET4-6 (0.4072); C12KET3-5 (0.1856); C12KET4-2 (0.4072)
ISO10	C12KET5-7 (0.2957); C12KET5-3 (0.2955); C12KET6-4 (0.2044); C12KET6-8 (0.2044)
ISO11	C12O5-7 (0.3195); C12O3-5 (0.3680); C12O4-6 (0.3125)
ISO12	C12O4-7 (0.4345); C12O3-6 (0.5655)
ISO13	C12H24-5 (0.1576); C12H24-3 (0.3345); C12H24-4 (0.5079)

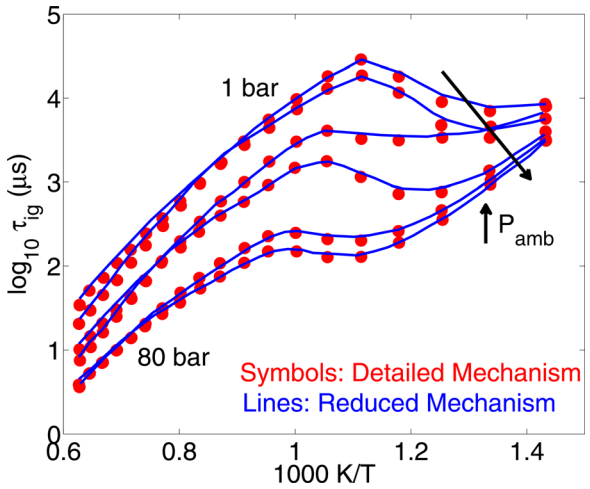

Fig. 9 Calculated ignition delay times for the SR23 mixture obtained using the detailed kinetic mechanism and the 163 species reduced mechanism at an equivalence ratio of 2

Table 2 Setup and boundary conditions for 3D spray combus-tion simulations obtained from measurements [24]

Parameter	Quantity
Fuels	SR23 *n*-dodecane
Nozzle outlet diameter	90 μm
Discharge coefficient	0.89
Fuel injection pressure	150 MPa
Fuel injection temperature	363 K
Injection duration	>4 ms
Injected fuel mass	19.7 mg
Injection rate shape	Square
Ambient gas temperature	800–1100 K
Ambient gas density	22.8 kg/m^3
Ambient O_2	15%

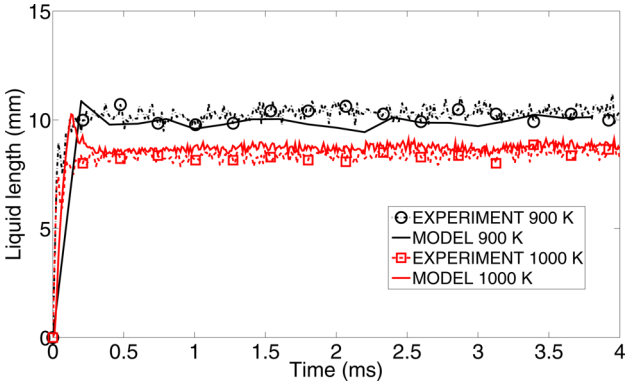

Fig. 10 Experimental [24] and computed liquid lengths at 900 and 1000 K ambient temperature conditions

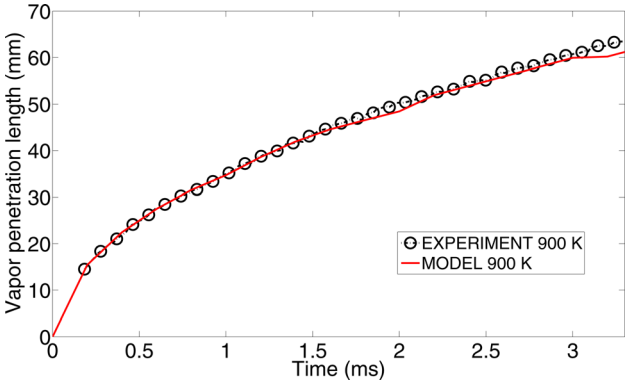

Fig. 11 Experimental [24] and computed vapor penetration lengths at 900 K ambient temperature condition

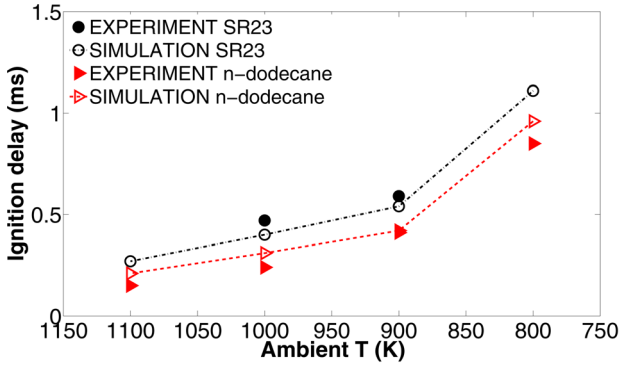

(a)

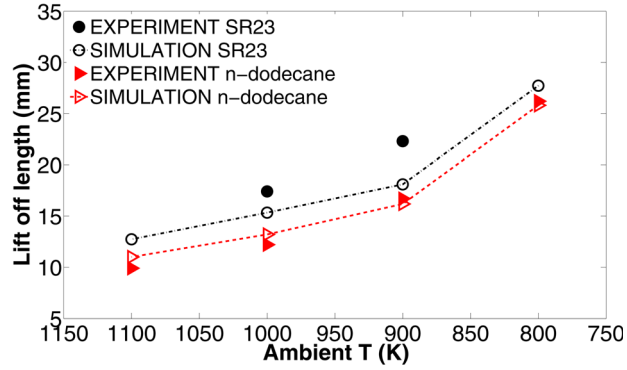

(b)

Fig. 12 Comparison of (*a*) ignition delay and (*b*) lift-off length for SR23 and *n*-dodecane from experiments [25] and simulations

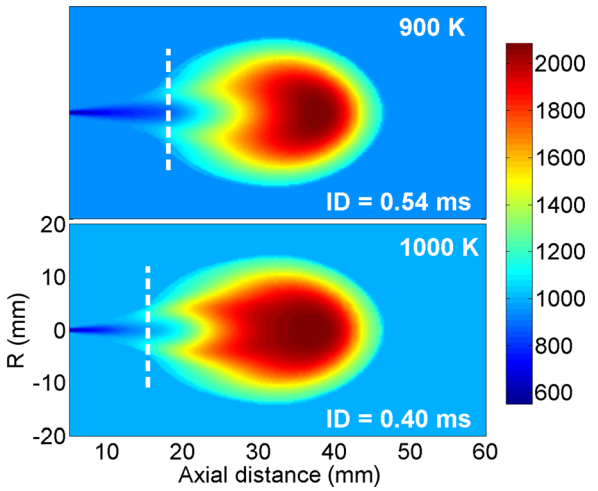

Fig. 13 Contour plots of temperature for 900 K and 1000 K conditions obtained from simulations at 1.5 ms for the SR23 mixture

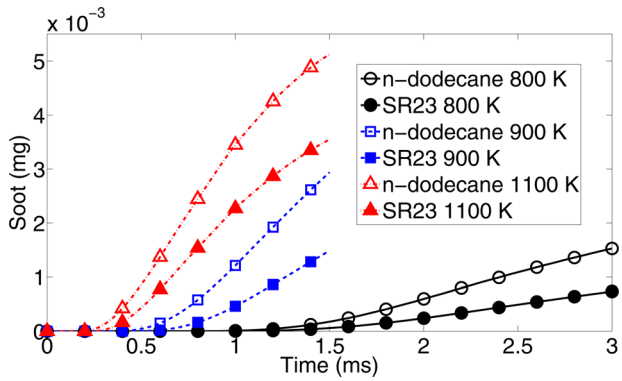

Fig. 14 Soot mass predictions versus time comparison for SR23 and *n*-dodecane at different ambient temperatures

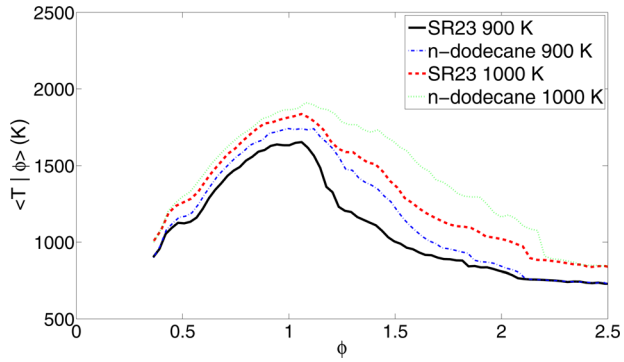

Fig. 16 Conditional average of temperature on equivalence ratio for SR23 and *n*-dodecane at 900 K and 1000 K ambient temperatures

enhanced with the SR23 mixture compared to *n*-dodecane, before the onset of combustion. However, the sensitivity to fuel composition going from one fuel surrogate to the other is clearly underpredicted. In future studies, we will focus on understanding whether the under prediction of the lift-off length is due to the spray characteristics or the chemical kinetic mechanism.

The presence of *m*-xylene slows the reactivity of the binary mixture as shown in Figs. 12(*a*) and 12(*b*). This allows for more entrainment of oxygen into the SR23 mixture compared to neat *n*-dodecane, yielding a leaner fuel/air equivalence ratio before the onset of combustion, which in turn reduces soot formation compared to neat *n*-dodecane [62]. On the other hand, it is also possible that the aromatic nature of xylene may promote soot formation [63]. This is examined in more detail in Fig. 14, which shows the soot mass predictions for SR23 and neat *n*-dodecane at different ambient temperatures. It is observed that the soot mass is significantly higher for neat *n*-dodecane than SR23 at different ambient temperatures. This indicates that although *m*-xylene may enhance soot production of SR23 due to its aromatic nature, the influence of enhanced fuel–air mixing characteristics (due to its longer ignition delay and lift-off length) are predominant, resulting in lower soot for SR23. This observation is in agreement with the experimental finding in Ref. [64] that cetane number, a measure for diesel fuels ignition properties, was found to play a major rule in soot emission of an optical single-cylinder CI engine.

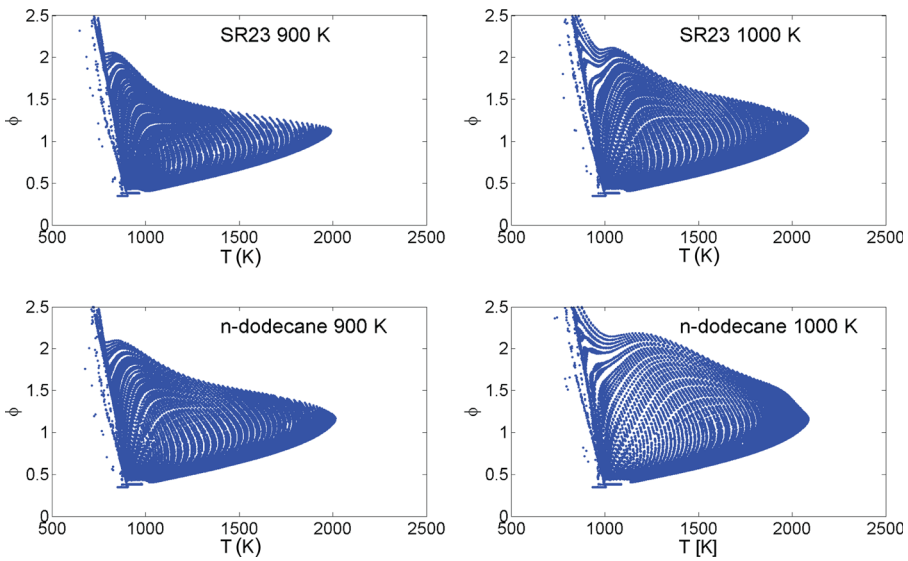

Fig. 15 Scatter plots of ϕ versus temperature in each of the computational cells for SR23 and *n*-dodecane cases at 900 and 1000 K ambient temperatures at 1.5 ms

To further understand the soot trends in Fig. 14, the equivalence ratio in temperature space is plotted in Fig. 15. The scatter plots of ϕ versus temperature at 1.5 ms for all the computational cells in the simulation are shown for SR23 and *n*-dodecane at 900 and 1000 K. It is observed from Fig. 15 that neat *n*-dodecane has greater regions of higher temperature in richer mixtures compared to SR23 at both ambient temperatures. Richer mixtures during ignition and combustion results in higher soot for *n*-dodecane, being consistent with the finding in Fig. 14. In order to further clarify the temperature regime in the rich mixture (e.g., high ϕ), averaged temperatures conditional on ϕ are plotted in Fig. 16 for both fuels. For a given temperature, the mixtures are richer for neat *n*-dodecane compared to SR23 which is consistent with the observations in Fig. 15.

5 Concluding Remarks

A skeletal mechanism of a multicomponent mixture of *n*-dodecane and *m*-xylene, with 163 species and 887 reactions was developed from a detailed mechanism consisting of 2885 species and 11,754 reactions for multidimensional diesel engine simulations. The parent xylene mechanism was presented and extensively validated using data from low and high temperature ignition, a jet stirred reactor, and spherically propagating flames. The combined mechanism for the binary surrogate mixture was also validated against available experimental data. Two rounds of DRG-X and DRGASA together with one round of isomer lumping were performed to obtain a reduced mechanism. The mechanism was validated against the detailed mechanism as well as available ST and flow reactor data. Overall, good agreement was observed for all the conditions. Further validation was conducted against a spray flame dataset from the ECN. It was found that the mechanism could capture the ignition delay very well, but slightly underpredicts the lift-off length, especially at lower ambient temperatures. Lower soot concentrations were predicted for SR23 at different ambient temperatures indicating that slow reactivity (i.e., enhanced fuel–air mixing) dominates the soot formation compared to the effect of *m*-xylene's aromatic nature.

Acknowledgment

The submitted manuscript has been created by UChicago Argonne, LLC, Operator of Argonne National Laboratory (Argonne). Argonne, a U.S. Department of Energy Office of Science laboratory, is operated under Contract No. DE-AC02-06CH11357. The U.S. Government retains for itself, and others acting on its behalf, a paid-up nonexclusive, irrevocable world-wide license in said article to reproduce, prepare derivative works, distribute copies to the public, and perform publicly and display publicly, by or on behalf of the Government.

The research was funded by DOEs Office of Vehicle Technologies, Office of Energy Efficiency and Renewable Energy under Contract No. DE-AC02-06CH11357. The authors wish to thank Gurpreet Singh, program manager at DOE, for his support. This work was also supported by the U.S. Department of Energy, Office of Basic Energy Sciences, Division of Chemical Sciences, Geosciences, and Biosciences, under Contract No. DE-AC02-06CH11357.

The work at UCONN was supported by the National Science Foundation and the Department of Energy through the NSF-DOE Partnership on Advanced Combustion Engines Program under Grant No. CBET-1258646.

The LLNL work was performed under the auspices of the U.S. Department of Energy by Lawrence Livermore National Laboratory under Contract No. DE-AC52-07NA27344 and was supported by the U.S. Department of Energy, Office of Vehicle Technologies (program manager Gurpreet Singh and Leo Breton).

We gratefully acknowledge the computing resources provided on "Fusion," a computing cluster operated by the Laboratory Computing Resource Center at Argonne National Laboratory.

The authors would also like to acknowledge Dr. R. Mandhapati, Mr. M. Wang, and Dr. P.K. Senecal from Convergent Science Inc. for providing technical supports and Dr. Marcia Huber at NIST for providing fuel property information.

References

[1] Lu, T., and Law, C. K., 2009, "Toward Accommodating Realistic Fuel Chemistry in Large-Scale Computations," Prog. Energy Combust. Sci., **35**(2), pp. 192–215.

[2] Luo, Z., Som, S., Sarathy, S. M., Plomer, M., Pitz, W. J., Longman, D. E., and Lu, T., 2014, "Development and Validation of an *n*-Dodecane Skeletal Mechanism for Spray Combustion Applications," Combust. Theory Model., **18**(2), pp. 187–203.

[3] Sarathy, S., Westbrook, C., Mehl, M., Pitz, W., Togbe, C., Dagaut, P., Wang, H., Oehlschlaeger, M., Niemann, U., Seshadri, K., Veloo, P. S., Ji, C., Egolfopoulos, F. N., and Lu, T., 2011, "Comprehensive Chemical Kinetic Modeling of the Oxidation of 2-Methylalkanes From C_7 to C_{20}," Combust. Flame, **158**(12), pp. 2338–2357.

[4] Mehl, M., Pitz, W., Westbrook, C., and Sarathy, S., 2011, "Chemical Kinetic Modeling of Substituted Aromatics," Fifth European Combustion Meeting (ECM2011), Cardiff University, Wales, UK, June 27-July 1.

[5] Westbrook, C. K., Pitz, W. J., Herbinet, O., Curran, H. J., and Silke, E. J., 2009, "A Comprehensive Detailed Chemical Kinetic Reaction Mechanism for Combustion of *n*-Alkane Hydrocarbons From *n*-Octane to *n*-Hexadecane," Combust. Flame, **156**(1), pp. 181–199.

[6] Mehl, M., Pitz, W. J., Westbrook, C. K., and Curran, H. J., 2011, "Kinetic Modeling of Gasoline Surrogate Components and Mixtures Under Engine Conditions," Proc. Combust. Inst., **33**(1), pp. 193–200.

[7] Brezinsky, K., Litzinger, T., and Glassman, I., 1984, "The High Temperature Oxidation of the Methyl Side Chain of Toluene," Int. J. Chem. Kinet., **16**(9), pp. 1053–1074.

[8] Emdee, J., Brezinsky, K., and Glassman, I., 1992, "A Kinetic Model for the Oxidation of Toluene Near 1200 K," J. Phys. Chem., **96**(5), pp. 2151–2161.

[9] Klotz, S. D., Brezinsky, K., and Glassman, I., 1998, "Modeling the Combustion of Toluene–Butane Blends," Proc. Combust. Inst., **27**(1), pp. 337–344.

[10] Sivaramakrishnan, R., Tranter, R., and Brezinsky, K., 2004, "High-Pressure, High-Temperature Oxidation of Toluene," Combust. Flame, **139**(4), pp. 340–350.

[11] Shen, H.-P. S., and Oehlschlaeger, M. A., 2009, "The Autoignition of C_8H_{10} Aromatics at Moderate Temperatures and Elevated Pressures," Combust. Flame, **156**(5), pp. 1053–1062.

[12] Roubaud, A., Lemaire, O., Minetti, R., and Sochet, L., 2000, "High Pressure Auto-Ignition and Oxidation Mechanisms of *o*-Xylene, *o*-Ethyltoluene, and *n*-Butylbenzene Between 600 and 900 K," Combust. Flame, **123**(4), pp. 561–571.

[13] Mittal, G., and Sung, C.-J., 2007, "A Rapid Compression Machine for Chemical Kinetics Studies at Elevated Pressures and Temperatures," Combust. Sci. Technol., **179**(3), pp. 497–530.

[14] Gaïl, S., and Dagaut, P., 2005, "Experimental Kinetic Study of the Oxidation of p-Xylene in a JSR and Comprehensive Detailed Chemical Kinetic Modeling," Combust. Flame, **141**(3), pp. 281–297.

[15] Johnston, R., and Farrell, J., 2005, "Laminar Burning Velocities and Markstein Lengths of Aromatics at Elevated Temperature and Pressure," Proc. Combust. Inst., **30**(1), pp. 217–224.

[16] Vasu, S. S., Davidson, D. F., Hong, Z., Vasudevan, V., and Hanson, R. K., 2009, "*n*-Dodecane Oxidation at High-Pressures: Measurements of Ignition Delay Times and OH Concentration Time-Histories," Proc. Combust. Inst., **32**(1), pp. 173–180.

[17] Natelson, R. H., Kurman, M. S., Johnson, R. O., Cernansky, N. P., and Miller, D. L., 2011, "Preignition and Autoignition Chemistry of the Xylene Isomers," Combust. Sci. Technol., **183**(9), pp. 897–914.

[18] Lu, T., Plomer, M., Luo, Z., Sarathy, S., Pitz, W., Som, S., and Longman, D., 2011, "Three Dimensional Simulations of Diesel Sprays Using *n*-Dodecane as a Surrogate," Fall Technical Meeting of the Eastern States Section of the Combustion Institute, Storrs, CT, Oct. 9-11.

[19] Liu, W., Sivaramakrishnan, R., Davis, M. J., Som, S., Longman, D., and Lu, T., 2013, "Development of a Reduced Biodiesel Surrogate Model for Compression Ignition Engine Modeling," Proc. Combust. Inst., **34**(1), pp. 401–409.

[20] Liu, W., Law, C. K., and Lu, T., 2009, "Multiple Criticality and Staged Ignition of Methane in the Counterflow," Int. J. Chem. Kinet., **41**(12), pp. 764–776.

[21] Liu, W., Kelley, A., and Law, C., 2010, "Flame Propagation and Counterflow Nonpremixed Ignition of Mixtures of Methane and Ethylene," Combust. Flame, **157**(5), pp. 1027–1036.

[22] Liu, W., Zhu, D., Wu, N., and Law, C. K., 2010, "Ignition of *n*-Heptane Pool by Heated Stagnating Oxidizing Flow," Combust. Flame, **157**(2), pp. 259–266.

[23] Kee, R., Rupley, F., Miller, J., Coltrin, M., Grcar, J., Meeks, E., Moffat, H., Lutz, A., Dixon-Lewis, G., and Smooke, M., 2000, "Chemkin Collection, Release 3.6," Reaction Design Inc., San Diego, CA.

[24] Kook, S., and Pickett, L. M., 2012, "Liquid Length and Vapor Penetration of Conventional, Fischer–Tropsch, Coal-Derived, and Surrogate Fuel Sprays at High-Temperature and High-Pressure Ambient Conditions," Fuel, **93**, pp. 539–548.

[25] Kook, S., and Pickett, L. M., 2012, "Soot Volume Fraction and Morphology of Conventional, Fischer-Tropsch, Coal-Derived, and Surrogate Fuel at Diesel Conditions," SAE Int. J. Fuels Lubr., **5**(2), pp. 647–664.

[26] Pickett, L., Bruneaux, G., and Payri, R., 2014, "Engine Combustion Network," Sandia National Laboratories, Livermore, CA, http://www.ca.sandia.gov/ecn

[27] Pei, Y., Hawkes, E. R., and Kook, S., 2013, "Transported Probability Density Function Modelling of the Vapour Phase of an *n*-Heptane Jet at Diesel Engine Conditions," Proc. Combust. Inst., **34**(2), pp. 3039–3047.

[28] Pei, Y., Hawkes, E. R., and Kook, S., 2013, "A Comprehensive Study of Effects of Mixing and Chemical Kinetic Models on Predictions of *n*-Heptane Jet Ignitions With the PDF Method," Flow Turbul. Combust., **91**(2), pp. 249–280.

[29] Xue, Q., Som, S., Senecal, P. K., and Pomraning, E., 2013, "Large Eddy Simulation of Fuel-Spray Under Non-Reacting IC Engine Conditions," Atomization Sprays, **23**(10), pp. 925–955.

[30] Xue, Q., Battistoni, M., Som, S., Quan, S., Senecal, P., Pomraning, E., and Schmidt, D., 2014, "Flame Lift-Off on Direct-Injection Diesel Fuel Jets: Oxygen Concentration Effects," SAE Int. J. Engines, **7**(2), pp. 1061–1072.

[31] Senecal, P., Pomraning, E., Richards, K., and Som, S., 2013, "An Investigation of Grid Convergence for Spray Simulations Using an LES Turbulence Model," SAE Paper No. 2013-01-1083.

[32] Bhattacharjee, S., and Haworth, D. C., 2013, "Simulations of Transient *n*-Heptane and *n*-Dodecane Spray Flames Under Engine-Relevant Conditions Using a Transported PDF Method," Combust. Flame, **160**(10), pp. 2083–2102.

[33] Pei, Y., Hawkes, E. R., Kook, S., Goldin, G. M., and Lu, T., 2015, "Modelling n-Dodecane Spray and Combustion With the Transported Probability Density Function Method," Combust. Flame, **162**(5), pp. 2006–2019.

[34] Egüz, U., Ayyapureddi, S., Bekdemir, C., Somers, B., and de Goey, P., 2013, "Manifold Resolution Study of the FGM Method for an Igniting Diesel Spray," Fuel, **113**, pp. 228–238.

[35] D'Errico, G., Lucchini, T., Contino, F., Jangi, M., and Bai, X.-S., 2013, "Comparison of Well-Mixed and Multiple Representative Interactive Flamelet Approaches for Diesel Spray Combustion Modelling," Combust. Theory Model., **18**(1), pp. 65–88.

[36] Abraham, J., and Pickett, L. M., 2010, "Computed and Measured Fuel Vapor Distribution in a Diesel Spray," Atomization Sprays, **20**(3), pp. 241–250.

[37] Bolla, M., Wright, Y. M., Boulouchos, K., Borghesi, G., and Mastorakos, E., 2013, "Soot Formation Modeling of *n*-Heptane Sprays Under Diesel Engine Conditions Using the Conditional Moment Closure Approach," Combust. Sci. Technol., **185**(5), pp. 766–793.

[38] Pei, Y., 2013, "Transported PDF Modelling of Spray Combustion at Practical Diesel Engine Conditions," Ph.D. thesis, The University of New South Wales, Sydney, Australia.

[39] Pei, Y., Kundu, P., Goldin, G. M., and Som, S., 2015, "Large Eddy Simulation of a Reacting Spray Flame Under Diesel Engine Conditions," SAE Paper No. 2015-01-1844.

[40] Pei, Y., Davis, M. J., Pickett, L. M., and Som, S., "Engine Combustion Network (ECN): Global Sensitivity Analysis of Spray A for Different Combustion Vessels," Combust. Flame (in press).

[41] Kösters, A., Karlsson, A., Oevermann, M., D'Errico, G., and Lucchini, T., 2015, "RANS Predictions of Turbulent Diffusion Flames: Comparison of a Reactor and a Flamelet Combustion Model to the Well Stirred Approach," Combust. Theory Model., **19**(1), pp. 81–106.

[42] Hawkes, E., Pei, Y., Kook, S., and Sibendu, S., 2013, "An Analysis of the Structure of an *n*-Dodecane Spray Flame Using PDF Modelling," Australian Combustion Symposium, Perth, Australia, Nov. 6–8, Paper No. F3-01.

[43] Payri, R., Viera, J. P., Pei, Y., and Som, S., "Experimental and Numerical Study of Lift-Off Length and Ignition Delay of a Two-Component Diesel Surrogate," Fuel (in press).

[44] Kundu, P., Pei, Y., Wang, M., Raju, M., and Som, S., 2014, "Evaluation of Turbulence Chemistry Interaction Under Diesel Engine Conditions With Multi-Flamelet RIF Model," Atomization Sprays, **24**(9), pp. 779–800.

[45] Chishty, M., Pei, Y., Hawkes, E., Bolla, M., and Kook, S., 2014, "Investigation of the Flame Structure of Spray-A Using the Transported Probability Density Function," 19th Australasian Fluid Mechanics Conference, Melbourne, Australia, Dec. 8-11, Paper No. 432.

[46] Pei, Y., Hawkes, E., and Kook, S., 2012, "Lagrangian–Lagrangian Modelling of an *n*-Heptane Jet at Diesel Engine Conditions," 18th Australasian Fluid Mechanics Conference, Launceston, Australia, Dec. 3–7, pp. 645–648.

[47] Pei, Y., Hawkes, E., and Kook, S., 2011, "Modelling *n*-Heptane Spray and Combustion in Conventional and Low-Temperature Diesel Engine Conditions," Aus-tralian Combustion Symposium, Newcastle, NSW, Australia, Nov. 29-Dec. 1, pp. 90–93.

[48] Convergent Science, 2013, "CONVERGE 2.1.0 Theory Manual," Convergent Science Inc., Middleton, WI.

[49] Reitz, R., and Diwakar, R., 1987, "Structure of High-Pressure Fuel Sprays," SAE Paper No. 870598.

[50] Huber, M., 2013, personal communication.

[51] Reitz, R. D., 1987, "Modeling Atomization Processes in High-Pressure Vaporizing Sprays," Atomisation Spray Technol., **3**(4), pp. 309–337.

[52] Patterson, M. A., and Reitz, R. D., 1998, "Modeling the Effects of Fuel Spray Characteristics on Diesel Engine Combustion and Emission," SAE Paper No. 980131.

[53] Schmidt, D. P., and Rutland, C., 2000, "A New Droplet Collision Algorithm," J. Comput. Phys., **164**(1), pp. 62–80.

[54] Frossling, N., 1958, "Evaporation, Heat Transfer, and Velocity Distribution in Two-Dimensional and Rotationally Symmetrical Laminar Boundary-Layer Flow," National Advisory Committee for Aeronautics, Washington, DC, NACA Technical Memorandum 1432.

[55] Liu, A. B., Mather, D., and Reitz, R. D., 1993, "Modeling the Effects of Drop Drag and Breakup on Fuel Sprays," SAE Paper No. 930072.

[56] Han, Z., and Reitz, R. D., 1995, "Turbulence Modeling of Internal Combustion Engines Using RNG κ-ε Models," Combust. Sci. Technol., **106**(4–6), pp. 267–295.

[57] Hiroyasu, H., and Kadota, T., 1976, "Models for Combustion and Formation of Nitric Oxide and Soot in Direct Injection Diesel Engines," SAE Paper No. 760129.

[58] Nagle, J., and Strickland-Constable, R., 1962, "Oxidation of Carbon Between 1000–2000 °C," *Proceedings of the Fifth Conference on Carbon*, University Park, PA, June 19-23, 1961, Pergamon, Oxford, UK, pp. 154–164.

[59] Pitsch, H., Chen, M., and Peters, N., 1998, "Unsteady Flamelet Modeling of Turbulent Hydrogen–Air Diffusion Flames," Proc. Combust. Inst., **27**(1), pp. 1057–1064.

[60] Hawkes, E., Pei, Y., Angelberger, C., and Bardi, M., 2012, "Ignition and Lift-Off Length," 2nd International Workshop of the Engine Combustion Network (ECN2), Heidelberg, Germany, Sept. 7-8.

[61] Somers, L., 2014, personal communication.

[62] Nikanjam, M., 1993, "Development of the First CARB Certified California Alternative Diesel Fuel," SAE Paper No. 930728.

[63] Glassman, I., 1989, "Soot Formation in Combustion Processes," Proc. Combust. Inst., **22**(1), pp. 295–311.

[64] Dumitrescu, C. E., Polonowski, C., Fisher, B. T., Cheng, A. S., Lilik, G. K., and Mueller, C. J., 2014, "An Experimental Study of Diesel-Fuel Property Effects on Mixing-Controlled Combustion in a Heavy-Duty Optical CI Engine," SAE Paper No. 2014-01-1260.